

RESEARCH

Open Access



Fibro-adipogenic progenitor cells in skeletal muscle unloading: metabolic and functional impairments

Margarita Sorokina^{1*}, Danila Bobkov^{1,2}, Natalia Khromova¹, Natalia Vilchinskaya³, Boris Shenkman³, Anna Kostareva^{1,4} and Renata Dmitrieva^{1*}

Abstract

Background Skeletal muscle resident fibro-adipogenic progenitor cells (FAPs) control skeletal muscle regeneration providing a supportive role for muscle stem cells. Altered FAPs characteristics have been shown for a number of pathological conditions, but the influence of temporary functional unloading of healthy skeletal muscle on FAPs remains poorly studied. This work is aimed to investigate how skeletal muscle disuse affects the functionality and metabolism of FAPs.

Methods Hindlimb suspension (HS) rat model employed to investigate muscle response to decreased usage. FAPs were purified from *m. soleus* functioning muscle (Contr) and after functional unloading for 7 and 14 days (HS7 and HS14). FAPs were expanded in vitro, and tested for: immunophenotype; in vitro expansion rate, and migration activity; ability to differentiate into adipocytes in vitro; metabolic changes. Crosstalk between FAPs and muscle stem cells was estimated by influence of medium conditioned by FAPs on migration and myogenesis of C2C12 myoblasts. To reveal the molecular mechanisms behind unloading-induced alterations in FAPs functionality transcriptome analysis was performed.

Results FAPs isolated from Contr and HS muscles exhibited phenotype of MSC cells. FAPs in vitro expansion rate and migration were altered by functional unloading conditions. All samples of FAPs demonstrated the ability to adipogenic differentiation in vitro, however, HS FAPs formed fat droplets of smaller volume and transcriptome analysis showed fatty acids metabolism and PPAR signaling suppression. Skeletal muscle unloading resulted in metabolic reprogramming of FAPs: decreased spare respiratory capacity, decreased OCR/ECAR ratio detected in both HS7 and HS14 samples point to reduced oxygen consumption, decreased potential for substrate oxidation and a shift to glycolytic metabolism. Furthermore, C2C12 cultures treated with medium conditioned by FAPs showed diverse alterations: while the HS7 FAPs-derived paracrine factors supported the myoblasts fusion, the HS14-derived medium stimulated proliferation of C2C12 myoblasts; these observations were supported by increased expression of cytokines detected by transcriptome analysis.

*Correspondence:
Margarita Sorokina
sorokinamy96@yandex.ru
Renata Dmitrieva
renata.i.dmitrieva@gmail.com

Full list of author information is available at the end of the article



© The Author(s) 2024. **Open Access** This article is licensed under a Creative Commons Attribution-NonCommercial-NoDerivatives 4.0 International License, which permits any non-commercial use, sharing, distribution and reproduction in any medium or format, as long as you give appropriate credit to the original author(s) and the source, provide a link to the Creative Commons licence, and indicate if you modified the licensed material. You do not have permission under this licence to share adapted material derived from this article or parts of it. The images or other third party material in this article are included in the article's Creative Commons licence, unless indicated otherwise in a credit line to the material. If material is not included in the article's Creative Commons licence and your intended use is not permitted by statutory regulation or exceeds the permitted use, you will need to obtain permission directly from the copyright holder. To view a copy of this licence, visit <http://creativecommons.org/licenses/by-nc-nd/4.0/>.

Conclusion the results obtained in this work show that the skeletal muscle functional unloading affects properties of FAPs in time-dependent manner: in atrophying skeletal muscle FAPs act as the sensors for the regulatory signals that may stimulate the metabolic and transcriptional reprogramming to preserve FAPs properties associated with maintenance of skeletal muscle homeostasis during unloading and in course of rehabilitation.

Keywords Soleus muscle, Functional unloading, Fibro-adipogenic progenitors (FAPs), C2C12 myoblasts, Skeletal muscle regeneration, Adipogenic differentiation, Cellular metabolism, Transcriptome analysis, FAPs-myoblasts interactions

Introduction

The population of skeletal muscle tissue-resident mesenchymal progenitor cells located between myofibers known as fibro-adipogenic progenitors (FAPs) is necessary to support skeletal muscle homeostasis and regeneration [1–4]. In response to acute injury, FAPs are activated, migrate to the site of injury, proliferate for several days, and then return to the basal level to avoid unnecessary accumulation of pathogenic FAPs [5]. The supportive role of FAPs in the maintenance of skeletal muscle stem cells (MuSCs) pool was confirmed with a wide number of cellular and animal models including inducible depletion of FAPs in a genetically modified mouse [6–8].

It was shown that in skeletal muscle FAPs utilize a transient pro-regenerative/pro-myogenic function *via* secreted factors, such as IL-6, WNT family members as well as a number of cytokines and growth factors [4, 9]. The exercise-induced signals influence FAPs paracrine function in healthy subjects [10, 11], and increase FAPs content in skeletal muscle of both humans [12] and mice [13]. Importantly, the changes in FAPs content correlated with alterations in MuSCs number, activity and changes in skeletal muscle adaptation to enhanced physical activity [12, 13]. Furthermore, there are data that the composition of FAPs is functionally heterogeneous and depends on the physiological context acting as the sensor and responder to the systemic and local changes in skeletal muscle homeostasis [14–18].

Our work provides evidence that FAPs can also sense the homeostatic perturbations caused by temporary functional unloading of skeletal muscle (i.e. space-flight, prolonged bed rest, cast immobilization). Most of detected alterations were unloading-time-dependent and can be divided into two categories: changes directly connected to the supporting role in the skeletal muscle growth/regeneration; and changes associated with unloading-induced metabolic reprogramming.

Methods

Hindlimb suspension rat model

Simulation of gravitational (functional) unloading of the rat hindlimbs was performed using hindlimb suspension (HS) model [19]. The use of this model induces characteristics similar to muscle atrophy. Therefore, this model

is used as the main method for simulating space flight and microgravity. In this work, we used this model for functional unloading of the *soleus* muscle (*m. soleus*) for 7 and 14 days.

Male Wistar rats (weighing 180 ± 5 g, 3-month-old) were randomly assigned to the following groups ($n=8$ /group): vivarium control (Contr), 7-day hindlimb suspension (HS7), and 14-day hindlimb suspension (HS14). The suspension height was adjusted to prevent the hindlimbs from touching any supporting surface while maintaining a suspension angle of approximately 30° . All animals were individually housed in a temperature-controlled room under a 12:12 h dark: light cycle with food pellets and water provided *ad libitum*. The *m. soleus* muscle was excised under isoflurane anesthesia using standardized dissection methods and weighed. Then, the rats were euthanized by decapitation under deep isoflurane anesthesia (4%). All procedures with the animals were approved by the Biomedicine Ethics Committee of the Institute of Biomedical Problems of the Russian Academy of Sciences/Physiology section of the Russian Bioethics Committee (protocol no. 581 and 582, 28.05.2021).

Skeletal muscle stem cells isolation

Fibro-adipogenic progenitors (FAPs) were isolated from *soleus* muscle enzymatically according to the protocols described previously [20] with minor changes.

Isolated muscles were placed into an enzyme solution, mechanically disrupted with scissors, and digested for 60 min at 37°C in 5 ml filtered 0.1% collagenase I (Sigma-Aldrich, Germany). Then, suspension was centrifuged for 5 min at 1000 g to remove collagenase and cell debris after digestion. Supernatant was discarded. For stem cells isolation from the fibers, the pellet was resuspended using sterile pipette tips in 2.5 ml of washing media (DMEM supplemented with 10% horse serum (Gibco, USA)). The pellet was pipetted for several minutes to isolate skeletal muscle stem cells from myofibrils and centrifuged (300 g, 5 min). The supernatant was transferred into a fresh tube. This procedure was performed twice. The double-collected supernatant was centrifuged for 10 min at 1000 g to discard debris. The supernatant was discarded, and the pellet of cells was placed in a proliferation media (DMEM supplemented with 1% penicillin-streptomycin, 1% L-glutamine, 1% chicken fetal serum

(USBiological, USA), 20% FBS (HyClone, USA), 10% horse-serum (Gibco, USA) on cell culture dishes.

The adhesion selection method was used to separate the population of fibro-adipogenic progenitors (FAPs). The suspension of cells was transferred to a culture dish without Geltrex and left in the incubator for 30–40 min, as described in the original article [21]. Fibro-adipogenic progenitors attached to the dish, while other cells remained in solution. For the expansion of the obtained FAPs was used a medium containing 10% FBS, 1% penicillin-streptomycin, 1% L-glutamine. Trypsin solution (2%) was used to dissociate FAPs from the dish.

Importantly, the *soleus* muscle is small and the volume of cellular samples that can be purified from each muscle/animal is not sufficient to perform the whole set of planned experiments with cells derived from one animal. Also, it is well documented that the quality of cellular samples may differ between sets of purification, and the long-term expansion of primary cultures in vitro causes substantial alterations in properties of primary cells. Therefore, at each experimental time point we combined samples derived from 8 animals before to start in vitro expansion to have FAPs samples big enough within 3–4 passages. This approach helped us to keep the culturing procedure uniform and maintain the consistent cellular phenotype in all samples.

Flow cytometry analysis

The immunophenotype of stem cells was evaluated by flow cytometry on CytoFLEX (Beckman Coulter). Freshly isolated FAPs were washed, resuspended in 100 μ l of PBS and incubated for 20 min at room temperature in the dark with the following antibodies (Ab): anti-PDGFR α -A488 (AI08115858, BIOSS), anti-CD45-PE (24264, BD Pharmingen), anti-Vimentin-FITC (AH032859, BIOSS), anti-CD73-PE (AH072347, BIOSS), anti-CD90-PE (22659, BD Pharmingen). Non-stained cells were used as negative control. Data were analyzed using the CytExpert 2.4 (Beckman Coulter) and Kaluza Analysis 2.1 software.

Adipogenic differentiation of FAPs

Adipogenic differentiation of FAPs was stimulated as described earlier [22] by replacing the culture media with adipocyte induction medium composed of culture medium supplemented with 1 μ M insulin, 1 μ M dexamethasone, and 0,5 μ M 3-isobutyl-1-methylxanthine. Differentiated adipocytes were fixed in 4% PFA and stained with Oil Red O at day 11 after induction according to the manufacturer's instructions (OilRed O Powder, Sigma). Hematoxylin and eosin staining was used for nucleus and cytoplasm visualization. Images from randomly chosen fields across several sections were acquired

using a fluorescent Zeiss Observer Z1 microscope with a TOUPCAM camera.

Pillow and OpenCV libraries in Python were used to quantify the area occupied by Oil Red O positive adipocytes. The number of fat droplets was estimated based on the percentage of red pixels in the images. First, the image was converted into HSV color space. Then, a mask was applied to the image and the percentage of light pixels was calculated.

RNA isolation, cDNA synthesis, and qPCR

Non-differentiated cells (day 0) and cells after 3 and 7 days of adipogenic differentiation were lysed with ExtractRNA kit (Evrogen, Russia). Concentration of RNA was measured with spectrophotometry using Nanodrop 3300 (Thermo Scientific, USA). Reverse transcription was performed from 500 ng RNA using Moloney Murine Leukemia Virus Reverse Transcriptase MMLV RT kit (Evrogen, Russia), according to instruction. qPCR was done using qPCRmix-HS SYBR+LowROX protocol (Evrogen, Russia). Primers for real-time PCR was designed via NSBI BLAST program. qPCR data are presented as arbitrary units of mRNA expression normalized to GAPDH house-keeping gene expression and to expression levels in the reference sample using $\Delta\Delta$ Ct method. Primer sequence can be provided upon request.

Statistical methods

Statistical analysis was performed using GraphPad Prism 8 software (GraphPad Software, USA, www.graphpad.com). Data were analyzed with a non-parametric Mann-Whitney test to determine significance. The criterion for statistical significance was $p < 0.05$ (* $p < 0.05$, ** $p < 0.01$, *** $p < 0.001$, **** $p < 0.0001$).

Bioenergetic analysis using seahorse technology

Cellular respiration of Contr and HS FAPs (7 and 14 days of functional unloading) was measured using Seahorse XFe24 Analyzer (Agilent Technologies, USA). Oxygen consumption rates (OCR) and extracellular acidification rates (ECAR) were measured in real-time. Bioenergetic analysis was performed on non-differentiated FAPs. 25×10^3 cells per well were seeded in a 24-well microplate (Agilent Technologies, USA). For cellular respiration we used Seahorse XF Cell Mito Stress Test standard protocol with a final concentration of 4 μ M Oligomycin, 5 μ M N5,N6-bis(2-fluorophenyl)-[1, 2, 5]oxadiazolo[3,4-b]pyrazine-5,6-diamine (BAM15), 2.5 μ M Rotenone and Antimycin A [16]. Data were normalized to the protein content. Each sample group included five replicates.

Based on OCR and ECAR results we calculated the respiration parameters: basal respiration, ATP production, spare respiratory capacity and OCR/ECAR ratio based

on S. Divakaruni article [23]. Statistical analysis was performed using GraphPad Prism.

RNA sequencing analysis

RNA sequencing analysis was performed on second-passage FAPs isolated from *m. soleus* muscle biopsies obtained from control rats (Contr) and rats under hindlimb suspension (7 and 14 days, HS7/HS14). Libraries for RNA sequencing were prepared using TruSeq Stranded mRNA kit (Illumina Inc., USA) according to the manufacturer manual. Libraries were quantified with 4150 TapeStation system (Agilent) using High Sensitivity DNA ScreenTape Analysis. Sequencing was performed on Illumina NextSeq 2000 (100 cycles). The quality of raw RNA-seq data was evaluated using the FastQC tool (v0.11.9). Then reads were mapped on rat genome using aligner STAR (v2.604a) with reference genome mRatBN7.2. Mapped reads were counted with the featureCounts program (v1.6.4) [24]. Alignment quality control was done with the MultiQC tool (v1.10.1). To determine gene patterns during the time course of functional unloading (0 days, 7 days and 14 days of hindlimb suspension), we used the LRT test (Likelihood ratio test). Differentially-expressed genes (DEGs) were determined using R package DESeq2 and filtered with $p_{adj} < 0.01$. Clusterization of identified DEGs was performed with the degPatterns function of the DEGreport package (version 1.28.0) to detect patterns of gene expression. The degPatterns function performs hierarchical clustering of samples based on pairwise correlations. Then, the hierarchical tree is cut to generate gene clusters. Number of clusters is chosen in such a way as to optimize the diversity of clusters (the variability between clusters should be greater than the variability within a cluster). Thus, this method allows to obtain clusters of genes with similar expression profiles. Genes of each cluster were further functionally annotated in Gene Ontology (Biological Process, Molecular Function, Cellular Component) terms and KEGG database using Gene Set Enrichment Analysis in clusterProfiler (version 3.14.3) R packages. Only signaling pathways with a $p_{adj} < 0.05$ were considered as statistically significant.

Raw fastq files and count tables are available at NCBI Gene Expression Omnibus database under the accession number GSE228869.

Collective migration analysis using scratch assay

FAPs or C2C12 myoblast cells were cultured in Dulbecco's modified Eagle's medium (DMEM, Gibco) supplemented with 10% of fetal bovine serum (FBS, Gibco), 1% penicillin-streptomycin, 1% L-glutamine. Cells were maintained at 37 °C in 5% CO₂. For the wound healing assay, cells were seeded at 24-well plate, incubated and allowed to grow for 24 h to reach 80–90% confluency. The

next day a scratch was made on a cell monolayer of FAPs/C2C12; C2C12 cell culture medium was replaced with FAPs conditioned medium in the second set of experiments. Then, cells were cultured for 24 h, and the wound area was automatically measured under an inverted phase-contrast microscope Image ExFluorer. The linear portion of the wound healing curve was selected for statistical tests using linear mixed effect model to examine the association between functional unloading and wound area. Model was adjusted for fixed effect (FAPs group and time points) and random effect (sample id). See figures legend for details.

Direct migration rate measuring

For migration analysis 20×10^3 cells per well were seeded in a 6-well microplate (Agilent Technologies, USA). The next day cells were visualized using Hoechst staining. FAPs migration rate was automatically measured under an inverted phase-contrast microscope Image ExFluorer. Cells were imaged every 15 min for 24 h. Tracks with a lasting time of more than 12 h were considered as valid.

Estimation of FAP's population doubling time

FAP's population expansion was performed using direct growth curve plotting. Initially, 20×10^3 cells were seeded in 6-well culture plates and cultured in an incubator at 37 °C and 5% CO₂. Cells were then trypsinized for 4 days and counted in a Neubauer chamber. For each cell group, three independent wells were analyzed. Then doubling time of the cell population was calculated.

C2C12 myogenic differentiation induced by FAPs-conditioned medium

Mouse myoblast C2C12 cell line was cultured in DMEM with 10% FBS, 1% penicillin-streptomycin, 1% L-glutamine. Then, cells were seeded in a 12-well cell plate and the next day cultured medium was replaced with medium conditioned for 24 h by FAPs (Contr, HS7 or HS14). Medium was changed every day. After 7 days of incubation in a conditioned medium, C2C12 formed myotubes.

Immunocytochemical staining

C2C12 myotubes were fixed in 4% paraformaldehyde for 15 min at room temperature and then permeabilized with 0.1% TritonX-100 for 5 min. Cells were then blocked with 10% FBS (Gibco) for 30 min and incubated with primary antibodies against myosin heavy chain (MF20, MAB4470, R&D Systems, USA). The secondary antibodies with Alexa Fluor 488 (Molecular Probes, USA) were applied for 45 min at room temperature. Nuclei were stained with DAPI (Molecular Probes, USA).

Measurement of fusion index and myotubes width

Fusion index and myotube width were determined at day 7 after replacement of growth medium to FAP's conditioned medium. For each experimental treatment, 10–13 digital images, with 5–10 myotubes on each photo, were captured with a fluorescent Zeiss Observer Z1 microscope. Myotubes with three and more nuclei per cell were used to calculate the fusion index and myotube's width. Fusion coefficient was calculated as a percent of nuclei incorporated in MF20 positive myotubes out of the total nuclei. Width of C2C12 myotubes under FAPs medium was measured with a fluorescent Zeiss Observer Z1 microscope. Data were presented as mean±SEM from three independent experiments. Differences between groups were tested for statistical significance using an unpaired Mann-Whitney test ($p < 0.05$ was considered as significant).

Results

Freshly isolated FAPs characterization

First, purified and expanded in vitro populations of FAPs derived from *m. soleus* muscle of control rats (Contr), and rats hindlimb suspended for 7 and 14 days (HS7/HS14) were tested for immunophenotype.

All samples showed similar morphology (data not shown), and mesenchymal CD90+/CD73+/VIM+/CD45-immunophenotype [25, 26], that did not differ significantly between Contr and HS samples (Supplemental Fig. 1). Importantly, in all samples the substantial fraction of cells was positive for PDGFR α (also known as CD140a), which is considered to be one of the key surface markers of FAPs [27, 28]; also, *Pdgfra* mRNA expression in FAPs samples did not differ between control and HS samples (Supplemental Fig. 2). Flow Cytometry data are summarized in Table 1. Together, these data indicate that the purification and in vitro expansion procedures affected FAPs samples in comparable ways.

Functional unloading affected FAPs in vitro expansion rate and migration activity in time-dependent manner

It is well known that upon injury or in response to exercise FAPs get activated to support skeletal muscle tissue repair and growth: they start to proliferate actively and migrate to the site of injury to create the supportive niche for skeletal muscle progenitors [2, 5, 29, 30].

Table 1 Flow cytometric analysis of freshly expanded fibro-adipogenic cells. The table shows the mean percentage of positive cells and SD value of two independent experiments

Marker	Contr FAPs, %	HS7 FAPs, %	HS14 FAPs, %
PDGFR α	61.98±10.02	62.58±7.49	60.49±8.18
Vimentin	96.16±3.10	96.28±5.12	95.64±4.98
CD90	97.30±2.01	96.67±1.71	93.24±5.48
CD73	96.45±3.72	96.66±4.75	95.85±5.08

To explore how functional unloading affects FAP's population expansion in vitro, and the ability to migrate we performed: scratch test assay (Fig. 1a, b), the direct measure of FAP's migration rate (Fig. 1c, d), evaluation of cellular population size over four passages (Fig. 1e), and calculation of the cellular population doubling time (Fig. 1f).

For the scratch test the wound area was automatically measured under an inverted phase-contrast microscope for 24 h, and the results were visualized with the trend line in the Fig. 1a (LOESS smoothing, confidence interval 95%). The linear mixed effect model analysis revealed the significant difference between HS14 and Control/HS7 curves ($p=0.013$) indicating the highest rate of wound healing in HS14 FAPs samples. Also, we calculated the wound area between 10 and 20 time points where the divergence between all three lines was more pronounced (Fig. 1b).

Since wound healing is a complicated dynamic process resulting from the cumulative effects of cellular proliferation and migration, we estimated migration rate and in vitro expansion separately. The quantitative analysis of direct automated tracking of cell migration (Fig. 1c) showed that HS14 FAPs have the highest migration rate, while the migration rate in HS7 sample was lower than in two others (Fig. 1d). On the contrary, the rate of in vitro expansion of HS7 FAPs determined by population size estimation and population doubling time calculation was the highest (Fig. 1e, f).

Together, these results show that the skeletal muscle functional unloading affects the properties of FAPs, and the alterations depend on the duration of unloading: it seems that at the day 7 FAPs were committed to proliferation while at later times (HS14) to migration. These data fit well the observed dynamics of wound healing: the migration activated in HS14 would contribute to the rapid infiltration of cells into the wound area doing the healing more effective; likewise, the increased rate of population doubling would also contribute to wound healing efficiency in HS7 samples as we could see at some points of healing process (Fig. 1a, b).

The ability of FAPs to differentiate into adipocytes in vitro is significantly altered by the skeletal muscle functional unloading

The ability of FAPs to differentiate into adipocytes in vivo and in vitro is well described [2, 3] and in pathological conditions excessive FAPs accumulation can be a cause of fibrosis and/or intramuscular fatty infiltration [30–32].

To estimate how hindlimb suspension affects the ability of FAPs to differentiate into adipocytes we stimulated adipogenic differentiation as described previously [22]. Upon stimulation all FAPs accumulated lipid droplets, but FAPs derived from functionally inactive muscles

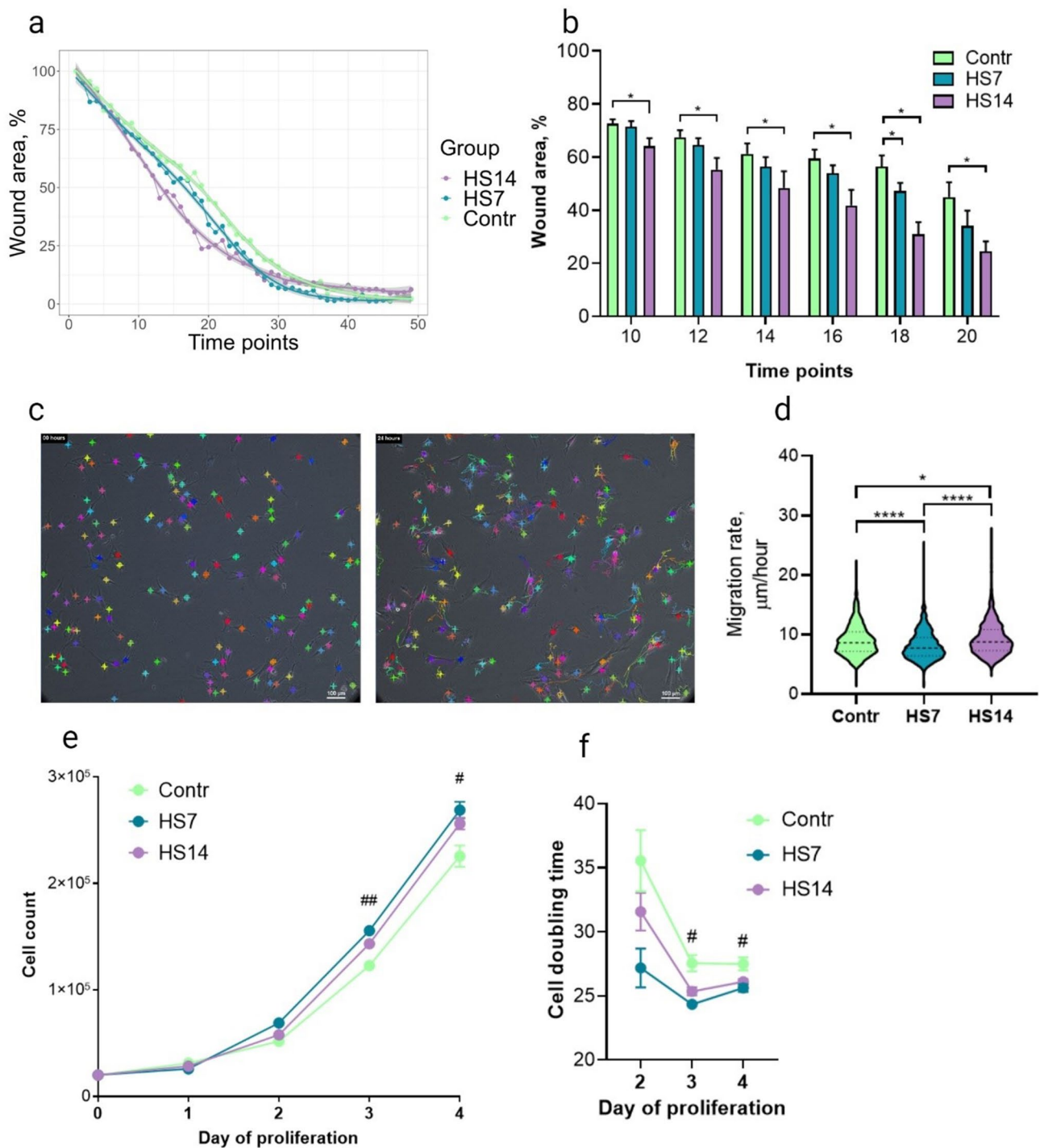


Fig. 1 Functional unloading affects FAP's expansion and migration activity of FAPs purified from *m. soleus* and expanded in vitro. **(a)** Wound healing dynamic: wound area was measured at indicated time points and normalized to area in time point 1. Data represented as mean value ($n=6$ biological replicates) and trend line shown in grey (95% confidence interval). **(b)** Wound area estimated at time points 10–20 and analyzed for HS and Control samples ($n=6$ biological replicates, $*p < 0.05$). **(c)** Representative tracing images of selected FAPs migration curves. **(d)** Migration rate of FAPs estimated from tracking images of individual cell ($n > 1000$, $*p < 0.05$, $****p < 0.0001$). **(e)** The dynamics of cellular growth of Contr/HS7/HS14 samples of FAPs between first and fourth passage. Data represented as mean \pm SEM ($n=3$ biological replicates, # show significant differences between HS7 and Contr samples, ## show significant differences in HS7 vs. Contr and HS14 vs. Contr comparisons). **(f)** FAPs population doubling times between second and fourth passages. Data represented as mean \pm SEM ($n=3$ biological replicates, # indicate significant differences between HS7 and Contr samples)

differentiated into adipocyte-like cells with a fewer number of lipid droplets that also were smaller in size than in Control FAPs. To visualize and quantify the adipogenic differentiation OilRed O staining was performed and images were analyzed: we have shown that ability of FAPs to accumulate fat decreased gradually depending on hindlimb suspension time (Fig. 2a-c).

We have also tested the expression of some specific markers of adipogenic progenitor's functionality: *Pparg*, *Fabp4*, *Atgl*, *Mgl1* (Fig. 2d-g). PPAR γ is the main regulator of adipogenesis; it regulates the transcription of a large number of genes involved in cell differentiation and lipid accumulation [33, 34]. Importantly, we identified significantly reduced mRNA level of the *Pparg* not only throughout adipogenic differentiation under HS condition, but also in non-stimulated FAPs at day 0 (Fig. 2d).

Also we have shown the decreased expression of *Fabp4* (Fatty acid binding protein, which binds long-chain fatty acids and primarily expressed in adipocytes [35])

(Fig. 2e), (Fig. 2e), *Atgl* and *Mgl1* (Adipose triglyceride lipase and Monoacylglycerol lipase both involved in the hydrolysis of triglycerides in adipocytes) (Fig. 2f, g) [36, 37]. Reduced expression of other adipogenesis - related genes that regulate glucose levels and fatty acid oxidation, such as, *Cebpa/b*, *Plin2*, *Ppargc1a* and *Adipoq* [38–42] was also detected in course of adipogenic differentiation of FAPs derived from functionally unloaded muscle (Supplemental Fig. 3).

Thus, these data indicate that skeletal muscle functional unloading turns down the ability of FAPs to accumulate large intracellular lipid droplets. The alteration in this fundamental characteristic of FAPs [6, 43] may point to unloading-induced metabolic reprogramming of FAPs; this hypothesis was further investigated.

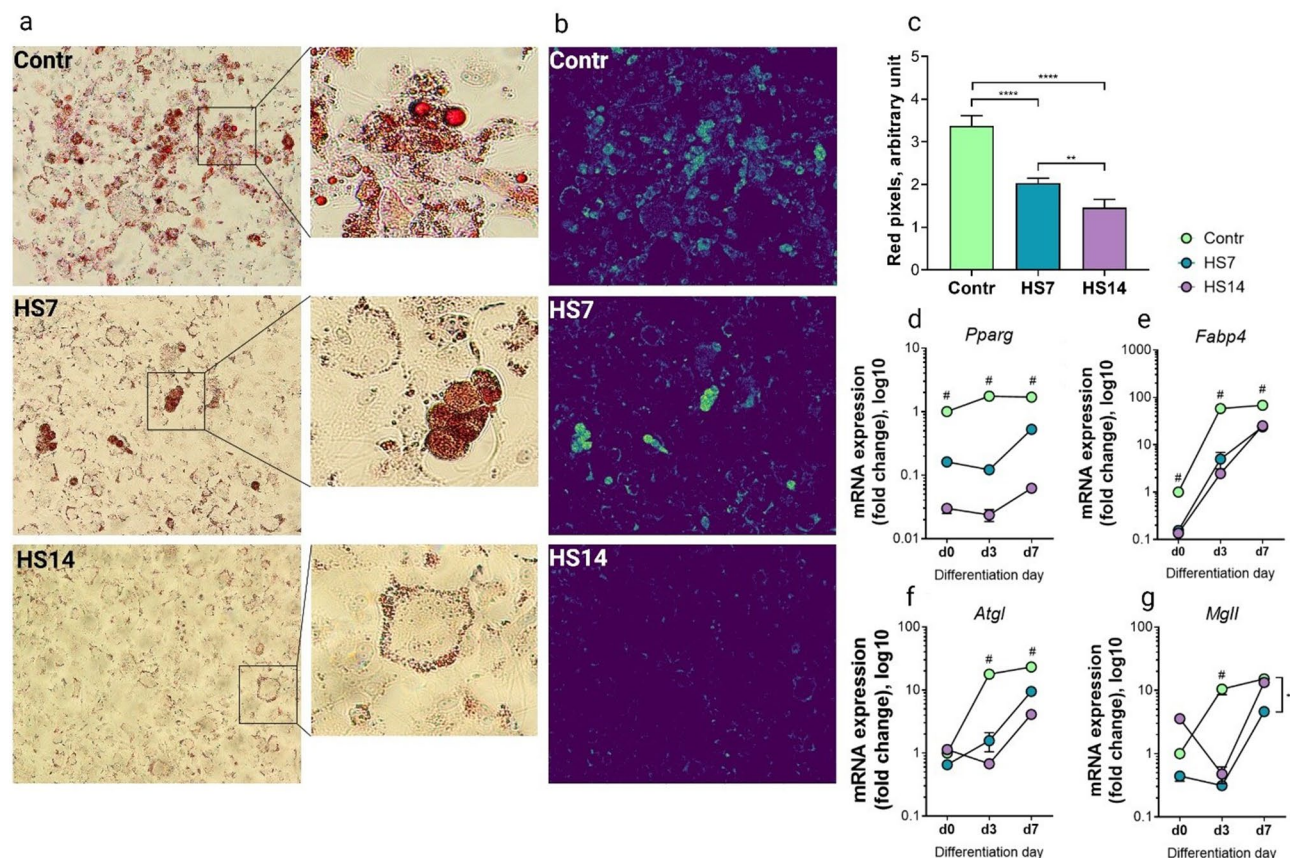


Fig. 2 Functional unloading affects adipogenic differentiation of FAPs in vitro. **(a)** Representative images of lipid droplets OilRed O staining performed on the 11th day after adipogenic stimulation (red). Hematoxylin and eosin staining were used for nucleus and cytoplasm visualization (magnification 20x). **(b)** Image mask that converts red pixels in original image to yellow color. Purple color – background. **(c)** Quantitative analysis of intracellular lipids accumulation. Image analysis in Python was performed to estimate a number of red-stained pixels, which correlates with the total volume fat droplets in the samples ($n=40$ technical replicates; ** $p < 0.01$, **** $p < 0.0001$). **(d-g)** qPCR analysis of key genes involved in adipogenic differentiation: *Pparg*, *Fabp4*, *Atgl*, *Mgl1*. Expression analysis was performed on non-differentiated FAPs (d0) and on 3 and 7 days after induction of adipogenic differentiation (d3 and d7); $n=4$ biological replicates; # show significant differences in HS7 vs. Contr and HS14 vs. Contr comparisons; * $p < 0.05$

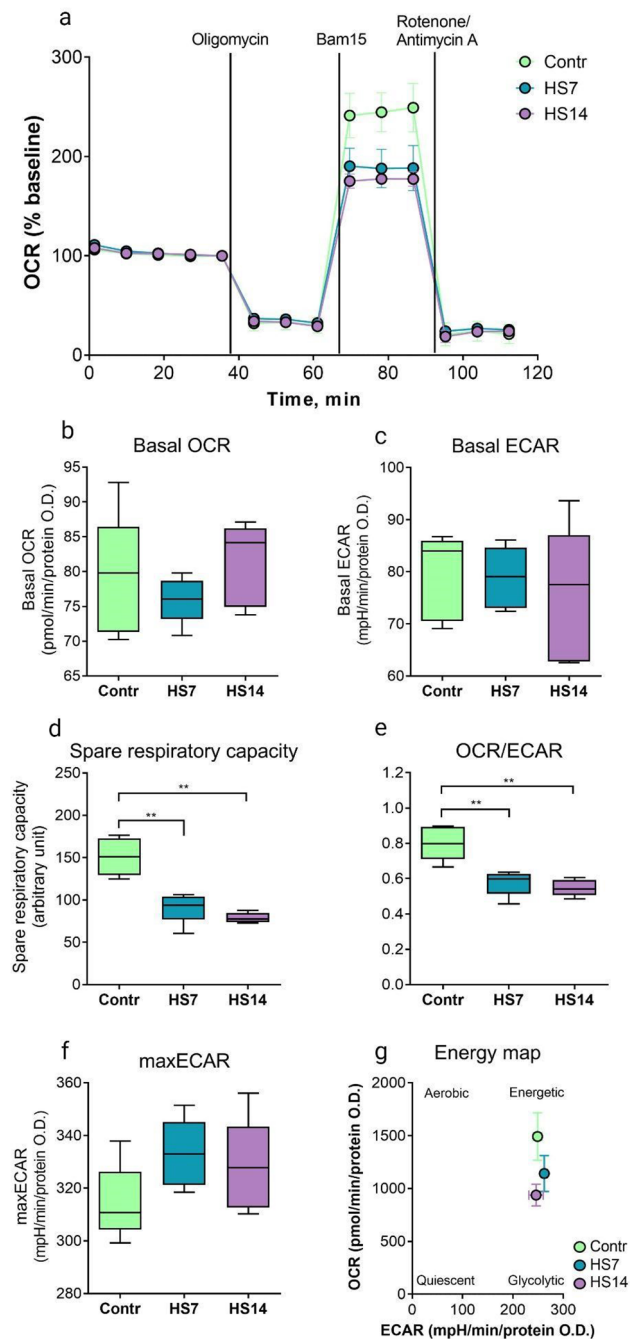


Fig. 3 Metabolic profiles and selected mitochondrial respiration parameters of FAPs isolated from control (Contr) muscle and after 7 and 14 days of hindlimb suspension (HS7 and HS14). **(a)** OCR traces for Contr, HS7 and HS14 group. Data were normalized to basal respiration and protein level **(b)** Basal OCR **(c)** Basal ECAR **(d)** Spare respiratory capacity **(e)** OCR/ECAR ratio. **(f)** Maximal ECAR **(g)** Energy map. HS7/HS14 FAPs exhibit a more glycolytic phenotype than Contr cells. Data were analyzed using Mann-Whitney test, $n=5$ biological replicates; ** $p<0.01$. Data presented as a box-and-whisker plot with min, median and max values

Skeletal muscle unloading results in metabolic reprogramming of FAPs

To test if skeletal muscle unloading causes metabolic reprogramming in FAPs we analyzed cellular bioenergetics using Seahorse technology. Mitochondrial Stress Test was performed for FAPs derived from functioning (Contr) muscle and functionally unloaded muscles HS7/HS14. The bioenergetics parameters were determined from real time oxygen consumption rate (OCR) profile (Fig. 3a) and extracellular acidification rate (ECAR) rate profile (Supplemental Fig. 4). The analysis showed no difference between all pairs of FAPs samples in both basal OCR (Fig. 3b) and basal ECAR (Fig. 3c), and ATP-linked O₂ consumption (data not shown). However, spare respiratory capacity, an important indicator of mitochondrial energetic status, significantly decreased in FAPs derived from HS7/HS14 muscles compared to control FAPs (Fig. 3d), which may indicate the adaptive response to decreased energy demands due to prolonged inactivity of suspended muscle [44].

In both HS7 and HS14 samples we detected the decreased OCR/ECAR ratio measured at the maximal OCR level (Fig. 3e). Also, we have shown the equal maxECAR rate in all samples (Fig. 3f). Furthermore, data visualized on an energy map graph (Fig. 3g) indicate that in the unloaded FAPs the mitochondria reduce oxygen consumption. Together, these data show that the relative contribution of glycolysis to the energy production increases in both HS7/HS14 FAPs, which can be considered as an unloading-induced shift to glycolytic metabolism.

FAPs conditioned medium affects wound healing and myogenic differentiation parameters in C2C12 myoblasts in unloading time-dependent manner

The simultaneous alterations in dynamics of FAPs population expansion, ability to migrate, accumulate lipid droplets, as well as metabolic reprogramming in response to the skeletal muscle functional unloading might result in the unloading-induced alterations in FAPs capability to support skeletal muscle homeostasis. We hypothesized that inactive (though healthy) muscle atrophying due to temporary unloading may produce signals to counteract atrophic changes and/or protect themselves from irreversible changes. Thus, FAPs can accept these signals and get “prepared” to provide support for skeletal muscle rehabilitation and growth when muscle activity begins to recover. Therefore, the next set of experiments was performed to test if FAPs - derived paracrine factors can modulate wound healing and myogenic differentiation in C2C12 myoblasts.

To assess how Contr/HS7/HS14 FAPs affect in vitro wound-healing we employed scratch test assay using proliferating C2C12 myoblasts cultured in medium

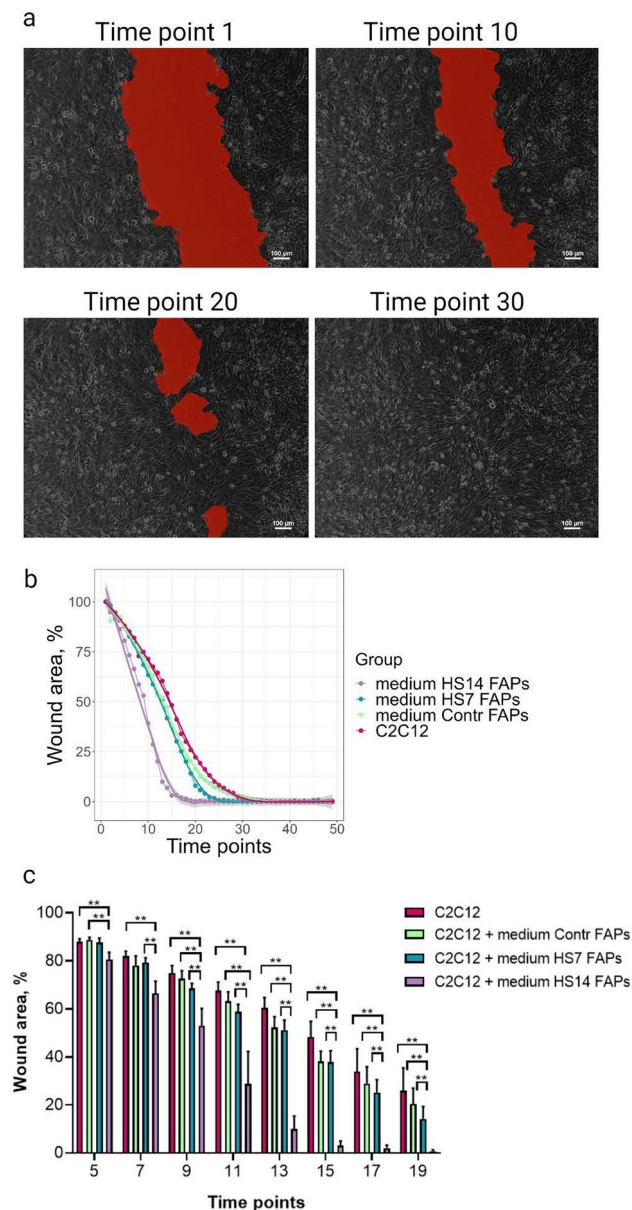


Fig. 4 C2C12 myoblasts wound healing and myogenic potential was changed under FAPs conditioned medium. **(a)** Representative wound images of C2C12 in time points: 1, 10, 20 and 30. The wound area was automatically measured by AI analysis (red color). Scale bar 100 μ m. **(b)** Wound healing dynamic of C2C12 under FAPs conditioned medium. Wound area was normalized to area in time point 1. Data represents the mean value (colored points, $n=6$ biological replicates) and trend line with 95% confidence interval (grey). **(c)** Wound area of C2C12 under FAPs conditioned medium (HS samples vs. Contr) calculated at 5–19 time points ($n=6$ biological replicates; $**p<0.01$). C2C12 cultured in standard media used as control condition

conditioned for 24 h by FAPs-derived paracrine factors (Fig. 4a). First, we have shown that in C2C12 cultures treated with medium conditioned by FAPs purified from HS14 *m. soleus* muscle the rate of in vitro wound healing increased significantly compared to cultures treated

with medium conditioned by FAPs purified from control and HS7 *m. soleus* muscle that showed wound healing rate similar to one in C2C12 myoblasts treated with regular culture medium. Linear mixed effect model also confirmed significant effect of HS14 medium on C2C12 wound healing ($p=0.00025$) (Fig. 4b). Also, the significantly increased wound healing rate of HS14 FAPs compared to Contr and HS7 samples was shown at 5–19 time points (Fig. 4c).

The final step of skeletal muscle differentiation in vivo is the formation of muscle fiber, the process that starts with myoblasts fusion. To test how FAPs-derived factors can modulate the fusion of myoblasts in our experimental model we treated sub-confluent (ready to differentiate) C2C12 myoblasts with medium conditioned by Contr/HS7/HS14 FAPs and have found that medium conditioned by FAPs derived from control and unloaded muscles stimulated myogenic differentiation of C2C12 myoblasts with different efficiency (Fig. 5a, b). In C2C12 cultures treated with HS14 medium the fusion activity of myoblasts was significantly lower than in two others (Fig. 4b); also, the width of myotubes in HS14 medium was smaller than in Contr/HS7 medium (Fig. 4c). The analysis of nuclei number fused into myotubes after stimulation with each of Contr/HS7/HS14 medium was performed and visualized as a density plot (Fig. 4d) and histogram (Fig. 4e). These data clarified the specific features of fusion in each condition: the numerous thin myotubes in HS14 medium were composed of 3–4 nuclei (more than 65%) while more than 60% of myotubes in HS7/Contr medium resulted from fusion of 5 and more nuclei with the substantial fraction of 15-and-more nuclei myotubes in HS7.

Together, these results may indicate that FAPs accept the signals from temporarily inactive skeletal muscle as the “instruction” to get prepared to perform their supportive work during skeletal muscle rehabilitation as soon as muscle activity is back to normal. It is interesting to note that these “instructions” showed the unloading time-dependent pattern: while the HS7 FAPs-derived paracrine factors supported the myoblasts fusion, the factors that stimulated myoblasts proliferation increased in HS14 medium.

RNA-seq analysis confirmed unloading-induced alterations in mechanisms that control FAPs metabolisms and regenerative potential

To reveal the molecular mechanisms behind alterations in FAPs functionality in the course of two weeks of hindlimb suspension we performed the analysis of transcriptome. The principal component analysis confirmed that FAPs samples were divided to specific groups according to experimental conditions (Supplemental Fig. 5). To visualize the patterns of “global”

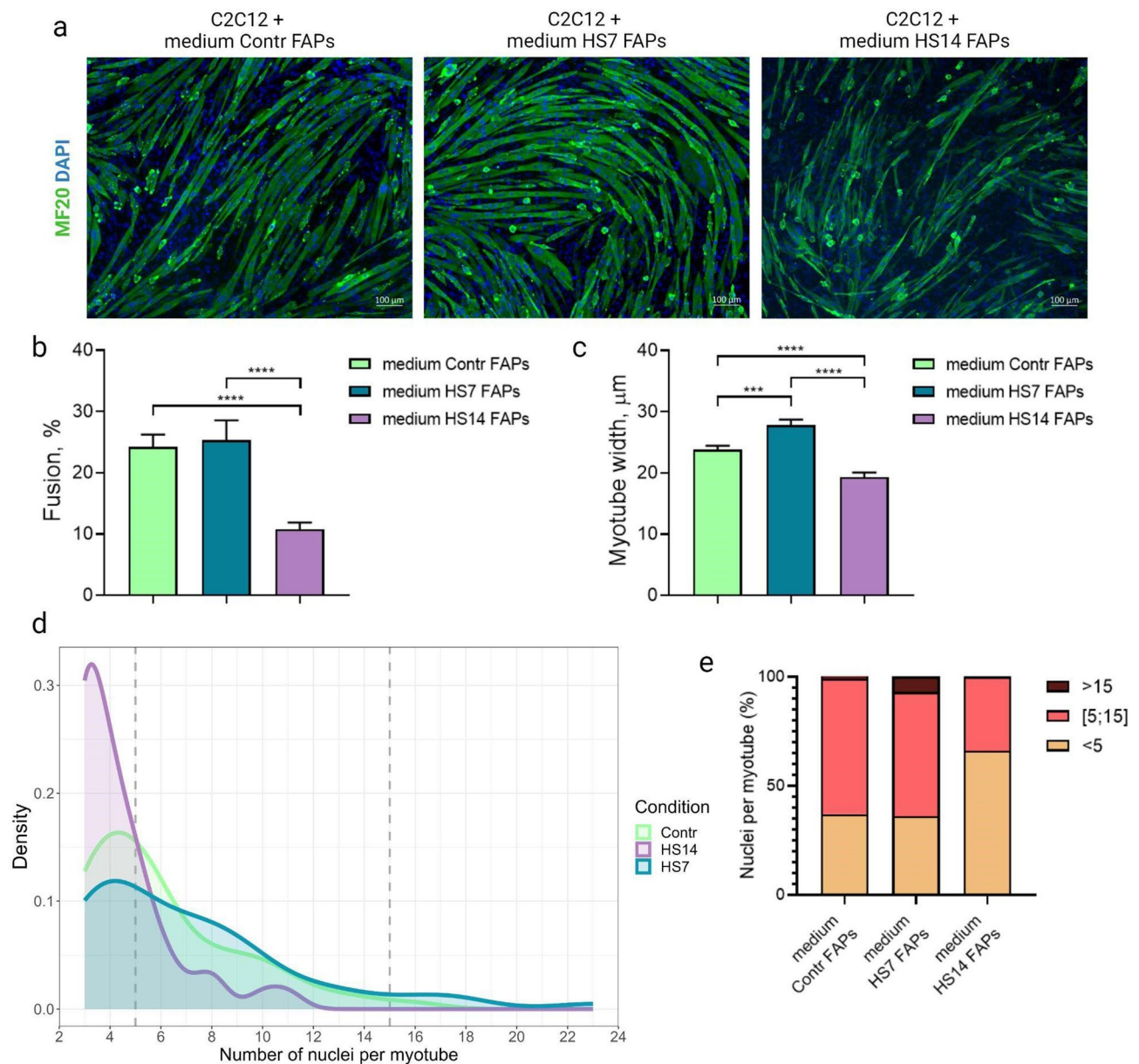


Fig. 5 C2C12 myoblasts myogenic potential was changed under FAPs conditioned medium (a) Immunocytochemical staining of myotubes on the 5th day of exposure of the FAPs conditioned medium on C2C12 cells. Myotubes are visualized using MF20 antibody to myosin-heavy-chain (MyHC, green). Nuclei are stained with DAPI (blue). Scale bar 100 μm . (b) Fusion coefficient is calculated as a percent of nuclei incorporated in MF20 positive myotubes ($n=13$ technical replicates, **** $p<0.0001$). Data presented as mean \pm SEM. (c) Width of C2C12 myotubes under FAPs medium (** $p<0.001$, **** $p<0.0001$). Data presented as mean \pm SEM. (d) A density plot of the number of nuclei per myotube. (e) Graphic representation of the contingency table of the number of nuclei in myotubes depending on the sample group: conditioned medium of Contr/HS7/HS14 FAPs

time-dependent alterations in molecular mechanisms that control FAPs functionality during hindlimb suspension we employed LRT test that allows to analyze the transcriptome changes during time course experiments to identify clusters of genes with similar expression patterns: the transition from the control muscle to HS7/HS14. Clusters of DEGs that show similar expression patterns were identified using the DEGreport package (Supplemental Table 1). Five clusters with at least 30 genes

with $p_{\text{adj}}<0.01$ each were identified (Fig. 6a). A functional analysis of signaling pathways was performed for genes from each cluster using the Gene Ontology database (Biological process, Cellular component, Molecular function) and KEGG database (Fig. 6b). The list of genes involved in corresponding signaling pathways is presented in Supplemental Table 2.

The expression of genes co-localized in cluster 1 was upregulated in HS7 samples, but slightly decreased in

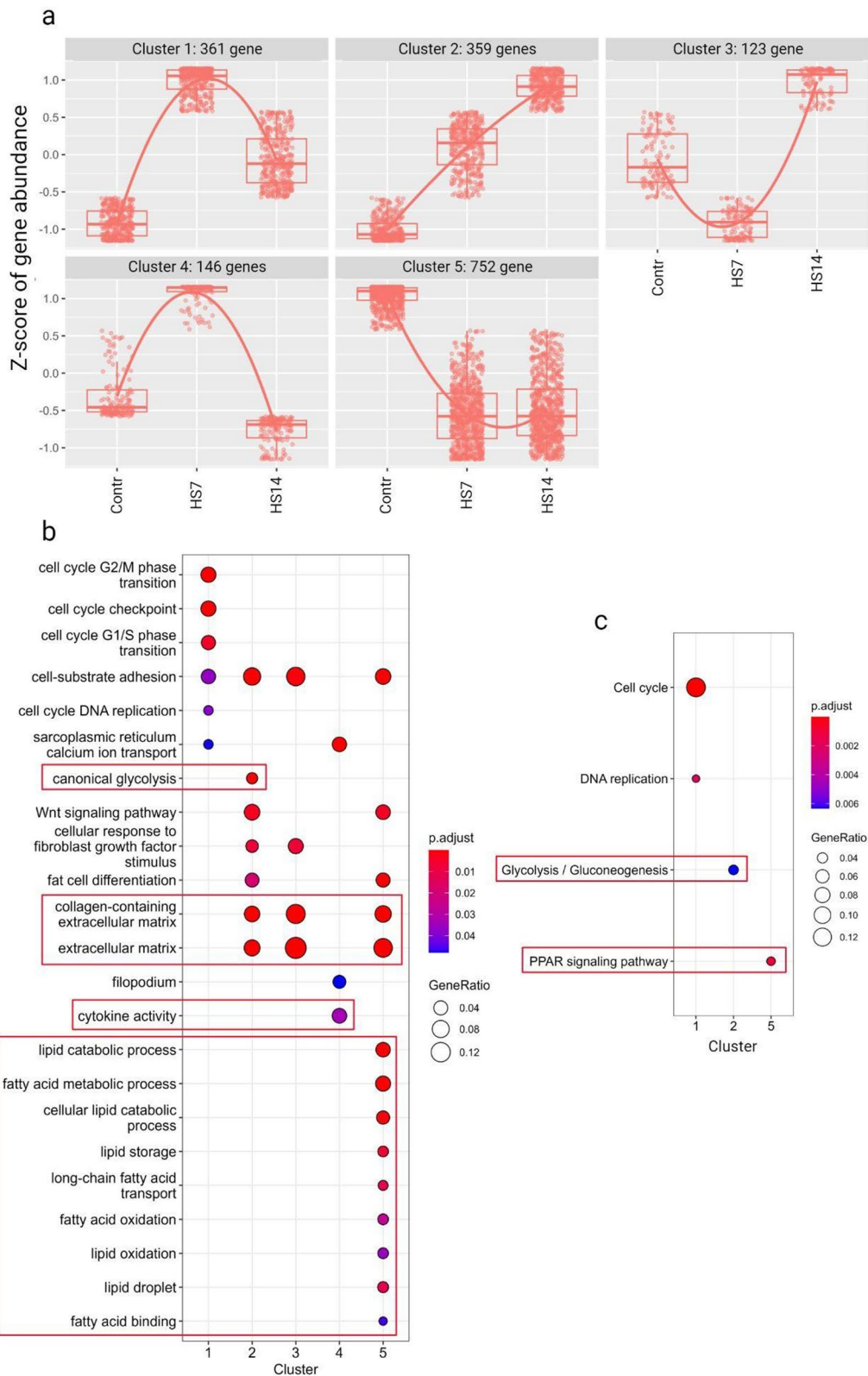


Fig. 6 Time-course transcriptomic analysis of FAPs during functional unloading: Contr – non unloaded FAPs, HS7 – hindlimb suspension during 7 days, HS14 – during 14 days. **(a)** Visualization of sets of DEGs that exhibit similar expression patterns across sample groups during hindlimb suspension. Five clusters with at least 30 genes with $p_{adj} < 0.01$ were identified. **(b)** Functional analysis of signaling pathways using the Gene Ontology database (Biological Process, Cellular Component, Molecular Function), $p_{adj} < 0.05$. **(c)** Functional analysis of signaling pathways using the KEGG database, $p_{adj} < 0.05$

HS14 samples; most of these genes belong to the pathways that control cell cycle (Fig. 6b,c), and this pattern correlates with the changes in FAPs proliferative activity we detected in functional experiments (Fig. 1e, f). The heatmap of genes in Cell cycle signaling pathway (from the KEGG database) is shown in the Supplemental Fig. 6 along with a brief description of the gene function.

The expression of genes in the second cluster gradually increased in the course of functional unloading (Fig. 6a). Genes in this cluster involved in control of key steps of canonical glycolysis: *Eno3* - key enzyme in the glycolytic pathway that catalyzes the conversion of 2-phosphoglycerate to phosphoenolpyruvate; *Pfkl* - catalyzes the major rate-limiting step in glycolysis, phosphorylation of D-fructose 6-phosphate to fructose 1,6-bisphosphate; *Pgk1* - catalyzes the conversion of 1,3-diphosphoglycerate to 3-phosphoglycerate; *Aldoa* - key enzyme in the fourth step of glycolysis/gluconeogenesis; *Pkm* - catalyzes the last, rate-limiting step, of glycolysis (Fig. 6b). Importantly, in the functional experiments we also detected the unloading-induced shift to the glycolytic metabolism in both HS7/HS14 FAPs (Fig. 3d, e).

The genes in the fourth cluster mapped to the cytokine activity pathway; the expression of these genes increased on the day 7 of functional unloading (HS7) and decreased substantially by the day 14 (HS14) (Fig. 6a, b). In this cluster were localized members of the CXC chemokine family, myokines *Cxcl1* [45] and *Cxcl4* [46], both involved in control of different steps of myogenesis and skeletal muscle homeostasis, adipokine *Cxcl3* also known to regulate the response of skeletal muscle stem cells to injury [47, 48]; another member of CXC chemokine family associated with this cluster is *Cxcl6*, shown to be upregulated in experiments aimed to study the muscle cells response to exercise using in vitro model with human primary myotubes [49]. Also, we identified in this cluster *Grem2* gene that modulates BMP signaling and known to inhibited adipogenesis in mesenchymal cells [50, 51], and *Wnt5a* gene that regulates muscle development mediating the activation of several noncanonical Wnt signaling pathways [52]. These data fit well the observations described above (Fig. 5) that the medium conditioned by HS7 FAPs stimulates myogenesis in C2C12 myoblasts better than medium conditioned by Contr/HS14 FAPs.

Most of the genes in the fifth cluster were mapped to signaling pathways that regulate the catabolism of lipids and fatty acids (Fig. 6b). Expression levels of these genes was decreased in both HS7 and HS14 FAPs samples; to specify the unloading-induced metabolic reprogramming we analyzed genes from cluster 5 using KEGG database, and PPAR signaling pathway, that plays a crucial role in both adipogenesis and energy expenditure, was found to be associated with these genes (Figs. 6c and 7). We have shown that the downregulated DEGs associated with

PPAR signaling pathway belong to practically all branches of PPAR-dependent signaling (Fig. 7c): *Hmgcs1* - responsible for the biosynthesis of ketone bodies, *Pltp* - lipid transfer protein, *Acsl3/5* - convert free long-chain fatty acids into fatty acyl-CoA esters, *Acox1* - first enzyme of the fatty acid beta-oxidation pathway, *Rxra* - forms heterodimers with PPARs, *Scp2* - involved in the oxidation of fatty acids, *Cpt1c* - regulates the beta-oxidation and transport of long-chain fatty acids into mitochondria, *Lpl* - catalyzes the hydrolysis of triglycerides, *Plin1/4* - coat intracellular lipid storage droplets, *Pparg* - key regulator of adipocyte differentiation and glucose homeostasis, *Fabp4* - uptake, transport, and metabolism of fatty acids, *Slc27a6* - uptake and transport of long-chain fatty acids. Heatmap of PPAR signaling pathway DEGs is shown in Fig. 7b. Thus, cluster analysis revealed extensive changes in the oxidation pathway of fatty acids and lipids in FAPs under the influence of functional unloading, and these data confirm our experimental results showing unloading-induced downregulation of ability to accumulate lipid droplets under adipogenic stimulation and decreased potential for substrate oxidation (Figs. 2 and 3).

Finally, it is recognized that a muscle-derived FAPs can differentiate into both adipocytes and fibrogenic cells. The pro-adipogenic pathways were associated exclusively with cluster 5 clearly indicating the decreased pro-adipogenic potential in the course of unloading. On the contrary, some genes associated with pro-fibrotic remodeling pathways (collagen-containing extracellular matrix, extracellular matrix pathways genes) were mapped to the clusters 2, 3, and 5 (Fig. 6b). The heatmap of genes in Extracellular matrix signaling pathway (Gene Ontology database) is shown in the Supplemental Fig. 7. These data indicate that there is no clear trend in pro-fibrotic activity in FAPs samples, and we suggest that the activation of FAPs-induced pro-fibrotic remodeling most likely does not occur in the healthy muscle functionally inactive over 2 weeks.

Discussion

The impact of altered FAPs content and functionality on pathological development of skeletal muscle fibrosis and/or fatty degeneration during aging, muscular dystrophy, and long-term inactivity due to spinal cord injury, paralysis or muscle denervation is well described [18, 53–59]. Also, it is known that in healthy subjects training-induced changes in FAPs content and paracrine activity contribute to the skeletal muscle stem cells adaptive response to exercise [10–13].

Most of the pathological conditions associated with decreased skeletal muscle activity, including aging [60, 61], Duchenne muscular dystrophy [62, 63], and other neuromuscular disorders [64, 65] cause the increase in FAPs adipogenesis associated with FAPs metabolic

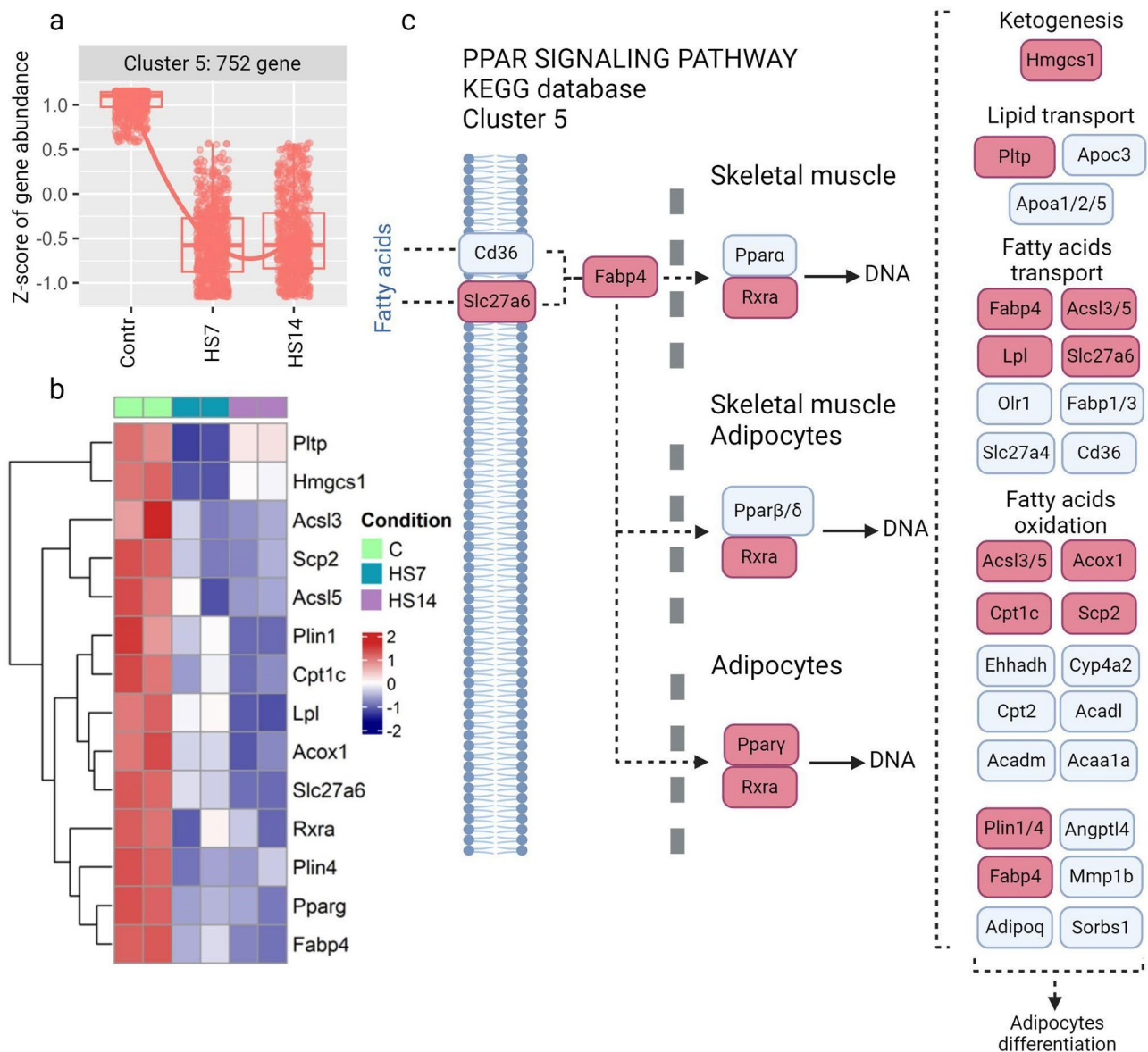


Fig. 7 Signaling pathway analysis of genes in cluster 5 using KEGG database **(A)** Gene expression profile during functional unloading **(B)** Heatmap of DEGs with $p_{\text{adj}} < 0.01$ in PPAR signaling pathway **(C)** Visualization of KEGG PPAR signal pathway. Downregulated genes in comparisons HS7 vs. Contr and HS14 vs. Contr are highlighted in red

reprogramming. Most of these diseases/conditions lead to progressive skeletal muscle wasting accompanied by fatty degeneration, and usually are untreatable and irreversible. In our work we investigated how the temporary unloading of healthy skeletal muscle causing the reversible skeletal muscle atrophy affects the FAPs functional properties including the ability to undergo adipogenic differentiation at least in vitro. The results we have obtained in this work allow us to speculate that intramuscular myofiber-to-FAPs cross-talks in the healthy muscle atrophying due to temporary unloading would cause alterations in FAPs functionality that differ from alterations caused by the cross-talks in diseased/aged muscle.

In this work we present new data on functional alterations in FAPs purified from healthy rat hindlimbs unloaded for 7 (HS7) and 14 (HS14) days and expanded in vitro. Most of detected alterations were unloading-time-dependent and can be divided into two categories: (i) changes directly connected to the supporting role in the skeletal muscle regeneration process; (ii) changes associated with unloading-induced metabolic reprogramming.

The ability of FAPs support muscle regeneration depends on FAPs-secreted growth factors and cytokines, or can be mediated *via* exosomal delivery of FAPs-derived factors that stimulate the proliferation

and differentiation of skeletal muscle progenitor cells (MuSCs). The role of FAPs-derived factors in tissue revascularization, extracellular matrix (ECM) remodeling, promotion of MuSCs migration to the injury site is also discussed in the literature [17, 66–68].

Our results obtained in functional experiments and supported by bioinformatic analysis were, in general, in line with the recognized evidence that activated FAPs support mechanisms associated with skeletal muscle regeneration and homeostasis. In this work we have shown that the cell culture medium conditioned by paracrine factors secreted by FAPs derived from unloaded muscle affected C2C12 myoblasts expansion, migration and differentiation in vitro. Importantly, FAPs-mediated effects were unloading-time-dependent: while the HS7-conditioned medium affected positively myotubes formation (Fig. 5), and the transcriptome analysis of HS7 samples showed the upregulation of pathway that regulate pro-myogenic cytokines activity, the HS14-conditioned medium downregulated C2C12 fusion coefficient, though stimulated C2C12 collective migration rate. Interestingly, our data show the time course similar to one obtained for injury-activated FAPs: the paracrine factors secreted by FAPs isolated from mouse muscles at day 3 post-acute injury, but not at day 15 significantly stimulated the formation myotubes in transwell co-culture system [18].

The diverged time course of FAPs functional properties (proliferation, migration, pro-myogenic cytokines activity) in our experiments can be explained from the following point of view: there are data on literature that the population of FAPs is dynamic, functionally heterogeneous, and the different subpopulations of FAPs depending on the physiological/pathological context may be present simultaneously in skeletal muscle tissue [16–18]. Therefore, we suggest that in course of unloading the progressively atrophying muscle may change the “request” for supportive action. As a result, FAPs may adopt their functionality to fit the new environmental circumstances following by the shift in the balance between functionally distinct FAPs subpopulations, and a new composition of secreted regulatory factors. It seems that at a certain time point of unloading the balance between atrophy-induced signals and FAPs response will be achieved until the restoration of physical activity and muscle contractions would give the signal to FAPs to re-activate the supporting activities in order to restore the muscle fiber volume.

Most of available data on FAP-associated metabolic reprogramming were obtained to resolve the mechanisms of skeletal muscle fibro-fatty degeneration in genetic disease, metabolic disorders, or aging [69]. Thus, in mouse model of Duchenne Muscular Dystrophy Reggio and co-authors have shown that mdx-derived FAPs have a higher in vitro adipogenic differentiation potential, reduced

mitochondrial ATP production and spare respiratory capacity, as well as more robust glycolytic flux than wild type matched cells [62]. On contrary, in our work we have shown, that FAPs isolated from the healthy unloaded *soleus* muscle possess the decreased ability to accumulate large lipid droplets in response to pro-adipogenic stimulation due to downregulation of signaling pathways that control early steps of adipogenesis and lipids metabolism including PPAR signaling (Figs. 2 and 6). The differences between results of Reggio’s work and our data fit well the theory that metabolic alterations play a crucial role in control of the stem cell fate in both physiological and pathological situations [70, 71]: while in dystrophic mdx-derived FAPs the enhanced glycolytic flux promoted the increase in sensitivity to pro-adipogenic stimulation, we have shown that in FAPs derived from unloaded healthy muscle the decrease in OXPHOS activity and reduced adipogenic differentiation in vitro (Fig. 3). Moreover, several studies showed that the regenerative microenvironment inhibits adipogenic differentiation and that FAPs proliferated in regenerating muscle without differentiating into adipocytes or fibroblasts [2, 3].

The molecular mechanisms behind changes associated with unloading-induced metabolic reprogramming of FAPs in healthy skeletal muscle remain to be clarified. In our work we showed unloading-induced downregulation of *Pparg* mRNA in FAPs (Fig. 2d), as well as downregulation of key genes in PPARγ-regulated pathways that control adipogenesis and lipid metabolic processes including lipolysis, beta-oxidation, and ketone body synthesis (Fig. 2 and Supplemental Fig. 3) [69]. We suggest the unloading-induced metabolic reprogramming is the part of molecular mechanisms activated to protect unloaded skeletal muscle from pathological changes associated with alterations in FAPs regulation and fatty degeneration. Indeed, there are data on literature that provide the support to this assumption: thus, Pagano and co-authors showed in physiological experiments that the muscle resting just after injury results in the substantial decrease in intermuscular adipose accumulation in regenerating tissue comparing to both injured/trained and just injured muscle [72]. Having in mind the fact that long-term (21 day) inactivity often results in intermuscular adipose accumulation that can be prevented by muscle activity [73], authors concluded, that the further studies are needed to determine the optimal time of necessary rest period for better recovery of skeletal muscle structure and functionality. Thus, we believe that our data can contribute to this field.

Study limitations

It is accepted that primary cell - based in vitro models of skeletal muscle growth, development and regeneration have their limitations. There are two main problems that

can affect results obtained from in vitro experiments: (i) in course of in vitro expansion without the supporting microenvironment cells tend to adapt to the new situation which may result in altered functionality; (ii) these models do not reflect all possible cell-to-cell interactions that can contribute to skeletal muscle functioning in vivo. To minimize or at least standardize the contribution of these factors we kept the uniform purification and culturing regimes to get the comparable cellular samples big enough to perform all planned experiments with the same sample. Thus, we had FAPs samples big enough to make a reasonable set of experiments within 3–4 passages of expansion. Also, to estimate the contribution of paracrine effects to myoblasts-myofiber-FAPs cross-talks we used the culture media conditioned by FAPs-derived paracrine factors. Obviously, all findings made with cultured cells should be verified using in vivo models, as well as the molecular mechanisms that protect these alterations in course of in vitro expansion.

Conclusion

To conclude, we suggest that the results obtained in this work show that the skeletal muscle functional unloading affects properties of FAPs in time-dependent manner: in atrophying skeletal muscle FAPs act as the sensors for the regulatory signals that may stimulate the metabolic and transcriptional reprogramming to preserve FAPs-mediated processes associated with maintenance of skeletal muscle homeostasis during unloading and in course of physical rehabilitation.

Abbreviations

Acox1	Acyl-CoA oxidase 1
Acs3/5	Acyl-CoA synthetase long chain family member 3/5
Adipoq	Adiponectin
Aldoa	Aldolase, fructose-bisphosphate A
Atgl (Pnpla2)	Patatin like phospholipase domain containing 2
ATP	Adenosine triphosphate
BAM15	N5,N6-bis(2-Fluorophenyl)-[1,2,5]oxadiazolo[3,4-b]pyrazine-5,6-diamine
BMP	Bone Morphogenetic Protein
CD45/73/90	Cluster of differentiation 45/73/90
Cebpa/b	CCAAT enhancer binding protein alpha/beta
Contr	Control group
Cpt1c	Carnitine palmitoyltransferase 1 C
Cxcl1/3/4/6	C-X-C motif chemokine ligand 1/3/4/6
DAPI	4',6-diamidino-2-phenylindole
DEGs	Differentially Expressed Genes
DMEM	Dulbecco's Modified Eagle Medium
ECAR	Extracellular acidification rate
ECM	Extracellular matrix
Eno3	Enolase 3
Fabp4	Fatty acid binding protein 4
FAPs	Fibro-adipogenic progenitors
FBS	Fetal bovine serum
Gapdh	Glyceraldehyde-3-phosphate dehydrogenase
Grem2	Gremlin 2, DAN family BMP antagonist
Hmgcs1	3-hydroxy-3-methylglutaryl-CoA synthase 1
HS	Hindlimb suspension
IL6	Interleukin 6
KEGG	Kyoto Encyclopedia of Genes and Genomes
LOESS	Locally estimated scatterplot smoothing

Lpl	Lipoprotein lipase
Mgll	Monoglyceride lipase
MSC	Mesenchymal stem cells
MuSCs	Muscle stem cells, satellite cells
OCR	Oxygen consumption rate
OXPPOS	Oxidative phosphorylation
PBS	Phosphate-buffered saline
Pdgfra	Platelet derived growth factor receptor alpha
PFA	Paraformaldehyde
Pfkfb3	Phosphofructokinase, liver type
Pgk1	Phosphoglycerate kinase 1
Pkm	Pyruvate kinase M1/2
Plin1/2/4	Perilipin 1/2/4
Pltp	Phospholipid transfer protein
PPAR	Peroxisome proliferator-activated receptors
Pparg	Peroxisome proliferator activated receptor gamma
Ppargc1a	PPARG coactivator 1 alpha
Rxra	Retinoid X receptor alpha
Scp2	Sterol carrier protein 2
Slc27a6	Solute carrier family 27 member 6
VIM	Vimentin
Wnt5a	Wnt family member 5 A

Supplementary Information

The online version contains supplementary material available at <https://doi.org/10.1186/s13395-024-00362-2>.

Supplementary Material 1

Supplementary Material 2

Supplementary Material 3

Acknowledgements

Authors thank Dr. A. Golovkin and Mr. A. Aquino for the help with Flow Cytometry analysis.

Author contributions

M.S. and R.D. conceptualized the project and wrote the manuscript. N.V. and B.S. organized, designed and performed animal experiments. M.S. performed all cell culture experiments, library preparation, sequencing and RNA-seq computational analysis. D.B. performed scratch tests and migration evaluation. R.D. and M.S. performed data analysis, interpretation and visualization. A.K. and N.K. secured funding and contributed to study coordination. R.D. supervised all of the work. All authors participated in project discussions and reviewed the manuscript. All authors have read and agreed to the published version of the manuscript.

Funding

This research was funded by the Russian Science Foundation grant no. 24-15-20006 (agreement 12.04.2024) and St. Petersburg Science Foundation no. 24-15-20006 (agreement 24.05.2024).

Data availability

The RNA-seq data is available in the NCBI Gene Expression Omnibus repository under the accession number GSE228869.

Declarations

Ethics approval and consent to participate

All procedures with animals in this study were approved by the Biomedicine Ethics Committee of the Institute of Biomedical Problems of the Russian Academy of Sciences/Physiology section of the Russian Bioethics Committee (protocol no. 581 and 582, 28.05.2021).

Consent for publication

Not applicable.

Competing interests

The authors declare no competing interests.

Author details

¹Almazov National Medical Research Centre, Saint Petersburg, Russia

²Institute of Cytology, Russian Academy of Sciences, Saint Petersburg, Russia

³Myology Laboratory, Institute of Biomedical Problems RAS, Moscow, Russia

⁴Department of Women's and Children's Health and Center for Molecular Medicine, Karolinska Institutet, Stockholm, Sweden

Received: 26 August 2024 / Accepted: 20 November 2024

Published online: 06 December 2024

References

1. Heredia JE, Mukundan L, Chen FM, Mueller AA, Deo RC, Locksley RM, et al. Type 2 innate signals stimulate fibro/adipogenic progenitors to facilitate muscle regeneration. *Cell*. 2013;153:376–88.
2. Joe AWB, Yi L, Natarajan A, Le Grand F, So L, Wang J, et al. Muscle injury activates resident fibro/adipogenic progenitors that facilitate myogenesis. *Nat Cell Biol*. 2010;12:153–63.
3. Uezumi A, Fukada S, Yamamoto N, Takeda S, Tsuchida K. Mesenchymal progenitors distinct from satellite cells contribute to ectopic fat cell formation in skeletal muscle. *Nat Cell Biol*. 2010;12:143–52.
4. Wosczyzna MN, Rando TA, A Muscle Stem Cell Support Group. Coordinated Cellular Responses in Muscle Regeneration. *Dev Cell* [Internet]. 2018;46:135–43. <https://doi.org/10.1016/j.devcel.2018.06.018>
5. Lemos DR, Babaeijandaghi F, Low M, Chang C-K, Lee ST, Fiore D, et al. Nilotinib reduces muscle fibrosis in chronic muscle injury by promoting TNF-mediated apoptosis of fibro/adipogenic progenitors. *Nat Med*. 2015;21:786–94.
6. Wosczyzna MN, Konishi CT, Perez Carbajal EE, Wang TT, Walsh RA, Gan Q, et al. Mesenchymal stromal cells are required for regeneration and Homeostatic Maintenance of Skeletal Muscle. *Cell Rep*. 2019;27:2029–e20355.
7. Fiore D, Judson RN, Low M, Lee S, Zhang E, Hopkins C, et al. Pharmacological blockage of fibro/adipogenic progenitor expansion and suppression of regenerative fibrogenesis is associated with impaired skeletal muscle regeneration. *Stem Cell Res*. 2016;17:161–9.
8. Uezumi A, Ikemoto-Uezumi M, Zhou H, Kurosawa T, Yoshimoto Y, Nakatani M et al. Mesenchymal Bmp3b expression maintains skeletal muscle integrity and decreases in age-related Sarcopenia. *J Clin Invest*. 2021;131.
9. Malecova B, Gatto S, Etxaniz U, Passafaro M, Cortez A, Nicoletti C et al. Dynamics of cellular states of fibro-adipogenic progenitors during myogenesis and muscular dystrophy. *Nat Commun* [Internet]. 2018;9:3670. <https://doi.org/10.1038/s41467-018-06068-6>
10. Boppart MD, De Lisio M, Zou K, Huntsman HD. Defining a role for non-satellite stem cells in the regulation of muscle repair following exercise. *Front Physiol*. 2013;4:310.
11. Collao N, Farup J, De Lisio M. Role of metabolic stress and Exercise in regulating Fibro/Adipogenic progenitors. *Front cell Dev Biol*. 2020;8:9.
12. Farup J, De Lisio M, Rahbek SK, Bjerre J, Vendelbo MH, Boppart MD, et al. Pericyte response to contraction mode-specific resistance exercise training in human skeletal muscle. *J Appl Physiol*. 2015;119:1053–63.
13. Valero MC, Huntsman HD, Liu J, Zou K, Boppart MD. Eccentric Exercise Facilitates Mesenchymal Stem Cell Appearance in Skeletal Muscle. *PLoS One* [Internet]. 2012;7:e29760. <https://doi.org/10.1371/journal.pone.0029760>
14. Yaseen W, Kraft-Sheleg O, Zaffryar-Eilol S, Melamed S, Sun C, Millay DP et al. Fibroblast fusion to the muscle fiber regulates myotendinous junction formation. *Nat Commun* [Internet]. 2021;12:3852. <https://doi.org/10.1038/s41467-021-24159-9>
15. Wei X, Nicoletti C, Puri PL. Fibro-Adipogenic progenitors: versatile keepers of skeletal muscle homeostasis, beyond the response to myotrauma. *Semin Cell Dev Biol*. 2021;119:23–31.
16. Farup J, Just J, de Paoli F, Lin L, Jensen JB, Billeskov T, et al. Human skeletal muscle CD90+ fibro-adipogenic progenitors are associated with muscle degeneration in type 2 diabetic patients. *Cell Metab*. 2021;33:2201–e221410.
17. Yao L, Tichy ED, Zhong L, Mohanty S, Wang L, Ai E, et al. Gli1 defines a subset of Fibro-adipogenic progenitors that promote skeletal muscle regeneration with less Fat Accumulation. *J bone Min Res off J Am Soc Bone Min Res*. 2021;36:1159–73.
18. Madaro L, Passafaro M, Sala D, Etxaniz U, Lugarini F, Proietti D et al. Denerivation-activated STAT3–IL-6 signalling in fibro-adipogenic progenitors promotes myofibres atrophy and fibrosis. *Nat Cell Biol* [Internet]. 2018;20:917–27. <https://doi.org/10.1038/s41556-018-0151-y>
19. Morey-Holton ER, Globus RK. Hindlimb unloading rodent model: technical aspects. *J Appl Physiol*. 2002;92:1367–77.
20. Smolina N, Kostareva A, Bruton J, Karpushev A, Sjöberg G, Sejersen T. Primary murine myotubes as a model for investigating muscular dystrophy. *Biomed Res Int*. 2015;2015.
21. Richler C, Yaffe D. The in vitro cultivation and differentiation capacities of myogenic cell lines. *Dev Biol*. 1970;23:1–22.
22. Dmitrieva RI, Minullina R, Bilibina AA, Tarasova OV, Anisimov SV, Zaritsky AY. Bone marrow- and subcutaneous adipose tissue-derived mesenchymal stem cells: differences and similarities. *Cell Cycle*. 2012;11:377–83.
23. Divakaruni AS, Paradyse A, Ferrick DA, Murphy AN, Jastroch M. Analysis and interpretation of microplate-based oxygen consumption and pH data [Internet]. 1st ed. *Methods Enzymol*. Elsevier Inc.; 2014. <https://doi.org/10.1016/B978-0-12-801415-8.00016-3>
24. Liao Y, Smyth GK, Shi W. featureCounts: an efficient general purpose program for assigning sequence reads to genomic features. *Bioinformatics*. 2014;30:923–30.
25. Dominici M, Le Blanc K, Mueller I, Slaper-Cortenbach I, Marini FC, Krause DS et al. Minimal criteria for defining multipotent mesenchymal stromal cells. The International Society for Cellular Therapy position statement. *Cytotherapy*. 2006.
26. Boxall SA, Jones E. Markers for characterization of bone marrow multipotential stromal cells. *Stem Cells Int*. 2012;2012.
27. Arrighi N, Moratal C, Clément N, Giorgetti-Peraldi S, Peraldi P, Loubat A, et al. Characterization of adipocytes derived from fibro/adipogenic progenitors resident in human skeletal muscle. 2015; Available from: www.nature.com/cddis
28. Contreras O, Rossi FMV, Theret M. Origins, potency, and heterogeneity of skeletal muscle fibro-adipogenic progenitors—time for new definitions. *Skeletal Muscle* [Internet]. 2021;11:16. <https://doi.org/10.1186/s13395-021-00265-6>
29. Contreras O, Cruz-Soca M, Theret M, Soliman H, Tung LW, Groppa E et al. Cross-talk between TGF- β and PDGFR α signaling pathways regulates the fate of stromal fibro-adipogenic progenitors. *J Cell Sci*. 2019;132.
30. Dammone G, Karaz S, Lukjanenko L, Winkler C, Sizzano F, Jacot G et al. PPAR γ Controls Ectopic Adipogenesis and Cross-Talks with Myogenesis During Skeletal Muscle Regeneration. *Int J Mol Sci* [Internet]. 2018;19. <https://www.mdpi.com/1422-0067/19/7/2044>
31. Pagano AF, Brioché T, Arc-Chagnaud C, Demangel R, Chopard A, Py G. Short-term disuse promotes fatty acid infiltration into skeletal muscle. *J Cachexia Sarcopenia Muscle*. 2018;9:335–47.
32. Buras ED, Converso-Baran K, Davis CS, Akama T, Hikage F, Michele DE et al. Fibro-Adipogenic Remodeling of the Diaphragm in Obesity-Associated Respiratory Dysfunction. *Diabetes* [Internet]. 2018;68:45–56. <https://doi.org/10.2337/db18-0209>
33. Ahmadian M, Suh JM, Hah N, Liddle C, Atkins AR, Downes M et al. PPAR γ signaling and metabolism: the good, the bad and the future. *Nat Med* [Internet]. 2013;19:557–66. <https://doi.org/10.1038/nm.3159>
34. Rosen ED, Sarraf P, Troy AE, Bradwin G, Moore K, Milstone DS, et al. PPAR gamma is required for the differentiation of adipose tissue in vivo and in vitro. *Mol Cell*. 1999;4:611–7.
35. Prentice KJ, Saksi J, Hotamisligil GS. Adipokine FABP4 integrates energy stores and counterregulatory metabolic responses. *J Lipid Res*. 2019;60:734–40.
36. Ojha S, Budge H, Symonds ME. Adipocytes in Normal Tissue Biology. In: McManus LM, Mitchell RNBT-P of HD, editors. San Diego: Academic Press; 2014. pp. 2003–13. <https://www.sciencedirect.com/science/article/pii/B9780123864567044087>
37. Nielsen TS, Møller N. Adipose triglyceride lipase and G0/G1 switch gene 2: approaching proof of concept. *Diabetes*. 2014;63:847–9.
38. Olofsson LE, Orho-Melander M, William-Olsson L, Sjöholm K, Sjöström L, Groop L, et al. CCAAT/enhancer binding protein alpha (C/EBPalpha) in adipose tissue regulates genes in lipid and glucose metabolism and a genetic variation in C/EBPalpha is associated with serum levels of triglycerides. *J Clin Endocrinol Metab*. 2008;93:4880–6.
39. Rosen ED, Hsu C-H, Wang X, Sakai S, Freeman MW, Gonzalez FJ, et al. C/EBPalpha induces adipogenesis through PPARgamma: a unified pathway. *Genes Dev*. 2002;16:22–6.

40. Takahashi Y, Shinoda A, Kamada H, Shimizu M, Inoue J, Sato R. Perilipin2 plays a positive role in adipocytes during lipolysis by escaping proteasomal degradation. *Sci Rep* [Internet]. 2016;6:20975. <https://doi.org/10.1038/srep20975>
41. Huang P-I, Chou Y-C, Chang Y-L, Chien Y, Chen K-H, Song W-S et al. Enhanced differentiation of three-gene-reprogrammed Induced Pluripotent Stem cells into adipocytes via adenoviral-mediated PGC-1 α overexpression. *Int J Mol Sci*. 2011. pp. 7554–68.
42. Abou-Samra M, Selvais CM, Dubuisson N, Brichard SM. Adiponectin and Its Mimics on Skeletal Muscle: Insulin Sensitizers, Fat Burners, Exercise Mimickers, Muscling Pills ... or Everything Together? *Int. J. Mol. Sci*. 2020.
43. Biferali B, Proietti D, Mozzetta C, Madaro L. Fibro-adipogenic progenitors cross-talk in skeletal muscle: the Social Network. *Front. Physiol. Frontiers Media S.A.*; 2019.
44. Nicholls DG. Spare respiratory capacity, oxidative stress and excitotoxicity. *Biochem Soc Trans*. 2009;37:1385–8.
45. Masuda S, Tanaka M, Inoue T, Ohue-Kitano R, Yamakage H, Muranaka K et al. Chemokine (C-X-C motif) ligand 1 is a myokine induced by palmitate and is required for myogenesis in mouse satellite cells. *Acta Physiol (Oxf)*. 2018;222.
46. Waldemer-Streyer RJ, Reyes-Ordoñez A, Kim D, Zhang R, Singh N, Chen J. Cxcl14 depletion accelerates skeletal myogenesis by promoting cell cycle withdrawal. *npj Regen Med* [Internet]. 2017;2:16017. <https://doi.org/10.1038/npjregenmed.2016.17>
47. Yahiaoui L, Gvozdic D, Danialou G, Mack M, Petrof BJ. CC family chemokines directly regulate myoblast responses to skeletal muscle injury. *J Physiol* [Internet]. 2008;586:3991–4004. <https://physoc.onlinelibrary.wiley.com/doi/abs/https://doi.org/10.1113/jphysiol.2008.152090>
48. Kusuyama J, Komorizono A, Bandow K, Ohnishi T, Matsuguchi T. CXCL3 positively regulates adipogenic differentiation. *J Lipid Res* [Internet]. 2016;57:1806–20. <https://www.sciencedirect.com/science/article/pii/S002227520353906>
49. Scheler M, Irmeler M, Lehr S, Hartwig S, Staiger H, Al-Hasani H, et al. Cytokine response of primary human myotubes in an in vitro exercise model. *Am J Physiol Cell Physiol*. 2013;305:C877–86.
50. Ali IHA, Brazil DP. Bone morphogenetic proteins and their antagonists: current and emerging clinical uses. *Br J Pharmacol* [Internet]. 2014;171:3620–32. <http://europepmc.org/abstract/MED/24758361>
51. Kawagishi-Hotta M, Hasegawa S, Igarashi T, Date Y, Ishii Y, Inoue Y et al. Increase of gremlin 2 with age in human adipose-derived stromal/stem cells and its inhibitory effect on adipogenesis. *Regen Ther* [Internet]. 2019;11:324–30. <https://www.sciencedirect.com/science/article/pii/S235232041930063X>
52. Asada N, Suzuki K, Sunohara M. Spatiotemporal distribution analyses of Wnt5a ligand and its receptors Ror2, Frizzled2, and Frizzled5 during tongue muscle development in prenatal mice. *Ann Anat - Anat Anzeiger* [Internet]. 2023;245:152017. <https://www.sciencedirect.com/science/article/pii/S0940960222001327>
53. Sastourné-Arrey Q, Mathieu M, Contreras X, Monferran S, Bourlier V, Gil-Ortega M et al. Adipose tissue is a source of regenerative cells that augment the repair of skeletal muscle after injury. *Nat Commun* [Internet]. 2023;14:80. <https://doi.org/10.1038/s41467-022-35524-7>
54. Fry CS, Johnson DL, Ireland ML, Noehren B. ACL injury reduces satellite cell abundance and promotes fibrogenic cell expansion within skeletal muscle. *J Orthop Res off Publ Orthop Res Soc*. 2017;35:1876–85.
55. Contreras O, Rebollo DL, Oyarzún JE, Olguín HC, Brandan E. Connective tissue cells expressing fibro/adipogenic progenitor markers increase under chronic damage: relevance in fibroblast-myofibroblast differentiation and skeletal muscle fibrosis. *Cell Tissue Res*. 2016;364:647–60.
56. Hamrick MW, McGee-Lawrence ME, Frechette DM. Fatty infiltration of skeletal muscle: mechanisms and comparisons with bone marrow adiposity. *Front Endocrinol (Lausanne)*. 2016;7:69.
57. Parker E, Hamrick MW. Role of fibro-adipogenic progenitor cells in muscle atrophy and musculoskeletal diseases. *Curr Opin Pharmacol* [Internet]. 2021;58:1–7. <https://www.sciencedirect.com/science/article/pii/S1471489221000230>
58. Moratal C, Arrighi N, Dechesne CA, Dani C. Control of muscle fibro-adipogenic progenitors by Myogenic Lineage is altered in aging and duchenne muscular dystrophy. *Cell Physiol Biochem Int J Exp Cell Physiol Biochem Pharmacol*. 2019;53:1029–45.
59. Ribeiro AF, Souza LS, Almeida CF, Ishiba R, Fernandes SA, Guerrieri DA, et al. Muscle satellite cells and impaired late stage regeneration in different murine models for muscular dystrophies. *Sci Rep*. 2019;9:1–11.
60. Lukjanenko L, Jung MJ, Hegde N, Perruisseau-Carrier C, Migliavacca E, Rozo M et al. Loss of fibronectin from the aged stem cell niche affects the regenerative capacity of skeletal muscle in mice. *Nat Med* [Internet]. 2016;22:897–905. <https://doi.org/10.1038/nm.4126>
61. Lukjanenko L, Karaz S, Stuelsatz P, Gurriaran-Rodriguez U, Michaud J, Damme G, et al. Aging disrupts muscle stem cell function by impairing Matricellular WISP1 secretion from Fibro-adipogenic progenitors. *Cell Stem Cell*. 2019;24:433–e4467.
62. Reggio A, Rosina M, Krahmer N, Palma A, Petrilli LL, Maiolatesi G et al. Metabolic reprogramming of fibro/adipogenic progenitors facilitates muscle regeneration. *Life Sci Alliance*. 2020;3.
63. Suárez-Calvet X, Fernández-Simón E, Natera D, Jou C, Pinol-Jurado P, Vil-lalobos E et al. Decoding the transcriptome of Duchenne muscular dystrophy to the single nuclei level reveals clinical-genetic correlations. *Cell Death Dis* [Internet]. 2023;14:596. <https://doi.org/10.1038/s41419-023-06103-5>
64. Chen W, You W, Valencak TG, Shan T. Bidirectional roles of skeletal muscle fibro-adipogenic progenitors in homeostasis and disease. *Ageing Res Rev* [Internet]. 2022;80:101682. <https://www.sciencedirect.com/science/article/pii/S1568163722001246>
65. Theret M, Rossi FMV, Contreras O. Evolving roles of muscle-Resident Fibro-Adipogenic progenitors in Health, Regeneration, Neuromuscular disorders, and aging. *Front Physiol*. 2021;12:673404.
66. Santini MP, Malide D, Hoffman G, Pandey G, D'Escamard V, Nomura-Kitabayashi A, et al. Tissue-Resident PDGFR α (+) progenitor cells contribute to Fibrosis versus Healing in a context- and Spatiotemporally Dependent Manner. *Cell Rep*. 2020;30:555–e5707.
67. Schultz E, Jaryszak DL, Valliere CR. Response of satellite cells to focal skeletal muscle injury. *Muscle Nerve*. 1985;8:217–22.
68. Davies MR, Garcia S, Liu M, Chi H, Kim HT, Raffai RL, et al. Muscle-derived Beige adipose precursors secrete promyogenic exosomes that treat Rotator Cuff muscle degeneration in mice and are identified in humans by single-cell RNA sequencing. *Am J Sports Med*. 2022;50:2247–57.
69. Giuliani G, Rosina M, Reggio A. Signaling pathways regulating the fate of fibro/adipogenic progenitors (FAPs) in skeletal muscle regeneration and disease. *FEBS J* [Internet]. 2022;289:6484–517. <https://febs.onlinelibrary.wiley.com/doi/abs/https://doi.org/10.1111/febs.16080>
70. Knobloch M, Pilz G-A, Ghesquière B, Kovacs WJ, Wegleiter T, Moore DL, et al. A fatty acid oxidation-dependent metabolic shift regulates adult neural stem cell activity. *Cell Rep*. 2017;20:2144–55.
71. Pala F, Di Girolamo D, Mella S, Yennek S, Chatre L, Ricchetti M et al. Distinct metabolic states govern skeletal muscle stem cell fates during prenatal and postnatal myogenesis. *J Cell Sci*. 2018;131.
72. Pagano AF, Arc-Chagnaud C, Brioché T, Chopard A, Py G. Muscle resting and TGF- β inhibitor treatment prevent fatty infiltration following skeletal muscle Injury. *Cell Physiol Biochem Int J Exp Cell Physiol Biochem Pharmacol*. 2019;53:62–75.
73. Pagano AF, Demangel R, Brioché T, Jublanc E, Bertrand-Gaday C, Candau R, et al. Muscle regeneration with Intermuscular Adipose Tissue (IMAT) Accumulation is modulated by mechanical constraints. *PLoS ONE*. 2015;10:e0144230.

Publisher's note

Springer Nature remains neutral with regard to jurisdictional claims in published maps and institutional affiliations.